Songklanakarin J. Sci. Technol.
31 (5), 533-540, Sep. - Oct. 2009

Songklanakarin Journal of Science and Technology
http://www.sjst.psu.ac.th

Original Article

Optimized baseplate geometry for ball swaging process by using finite element analysis

Pattaramon Jongpradist*, Rattharong Rojbunsongsri and Chatchapol Sukkana

Department of Mechanical Engineering, Faculty of Engineering,
King Mongkut's University of Technology Thonburi, Bangmod, Tung Khru, Bangkok, 10140 Thailand.

Received 24 April 2009; Accepted 19 September 2009

Abstract

A ball swaging process is commonly used in the hard disk drive manufacturing process to attach a suspension arm to an actuator arm via a part known as the baseplate. The geometry of the baseplate affects the contact pressure profile between the baseplate and the arm, torque retention of the swaged connection, and deformation of the assembly parts. In the current study, the effects of altering the baseplate geometric parameters on its characteristics are studied. A large-deformation dynamic finite element analysis of a ball swaging process is performed by using a commercial program ABAQUS. The products of combining several geometric parameters are also investigated so as to obtain the baseplate geometry with improved torque retention and reduced tilt angle. It is concluded that a proper design of the baseplate is in such way that the baseplate boss and the arm possess the largest contact area and that the stress concentration at the baseplate neck is minimal.

Keywords: ball swaging, baseplate, hard disk drive, torque retention, tilt angle, finite element analysis

1. Introduction

A ball swaging process is commonly used in the hard disk drive manufacturing process to attach a suspension arm to an actuator arm via a part known as the baseplate. The baseplate usually includes a thin flange and a sleeve called swage boss as shown in Figure 1. The flange of the baseplate is spot-welded to a suspension arm carrying a hard disk head slider. The swage boss is inserted into the corresponding swage openings of the suspension and the actuator arm. A cross-sectional view of the assembly is shown in Figure 2.

A swaging process starts with an insertion of the assembly into a swage device that applies clamping pressure to the assembly to prevent slippage of the parts during the process. A swage ball is then driven through the baseplate boss by a rigid pin and thus exerts a deforming load on the boss. Contact pressures, thereby frictional engagement, are generated between the outer surface of the boss and the inner

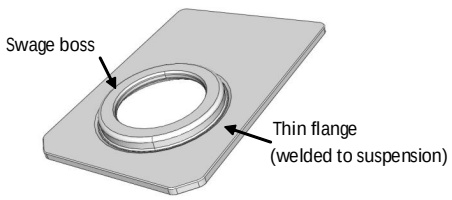

Figure 1. Components of the baseplate.

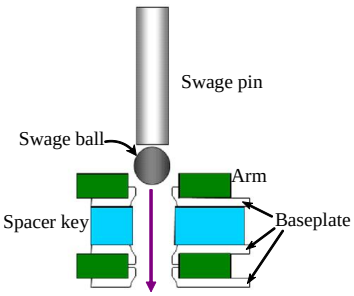

Figure 2. Cross-sectional view of the assembly for ball swaging process.

*Corresponding author.
Email address: pattaramon.tan@kmutt.ac.th

surface of the opening in the actuator arm. In other words, the swage boss creates an interference fit against the inner wall of the actuator arm opening. Accordingly, the assembly parts are firmly coupled to each other providing a connection with retention torque. However, high stresses occurring during the process can cause excessive deformation of the actuator arm. This leads to changes in the desired position and orientation of the suspension, known as z-height changes, and in the spring characteristics of the suspension, known as gram changes. Internal creep can cause stress relaxation of the material overtime such that the stress can be maintained at some lower level. In this case, the radial force will also decrease, possibly to the point where the frictional engagement is no longer enough to resist the operating torque. Although stress relaxation is not substantial for most materials operating at room temperature, a higher strain rate from an increased ball velocity could result in more relaxation and should be limited in the ball swaging process.

Kamnerdtong *et al.* (2005) studied the effects of swaging process parameters including the size, velocity, and shooting direction of the swage ball by using an axisymmetric finite element analysis. It was shown that the torque resistance was dominated by the contact pressure of the swaging process and that the unpleasant higher stress intensity in the necking zone of the baseplate resulted in higher deformation of the arm. Aoki and Aruga (2007) performed a three-dimensional large deformation analysis for ball swaging and concluded that the baseplate is influenced by the arm deformation due to asymmetric stress. Several recommendations had also been given regarding optimal baseplate dimensions (Zhang *et al.*, 2006; Zhang and Wolter, 2008) and changes of the baseplate figure by adding some auxiliary components (Boutaghou *et al.*, 1999; Kant *et al.*, 2000; Yim, 2002; Diewanit *et al.*, 2005) to advance the retention torque and diminish the gram load change. However, understanding on the influences of geometric changes of baseplate is still insufficient. Jongpradist *et al.* (2009) investigated the effects of changing geometry of the swage boss including its inner diameter, height, and chamfer angle at the top of the boss to the quality of the swaged connection. Recommendations on favorable values of each parameter were also proposed. Though, the products from combinations of various parameters are not examined. Also, influences of other geometric parameters of the baseplate have not yet been observed. The current research is an extension of this work to amend the lack of understanding in these issues, in which effects of other geometric parameters are studied and an optimized geometry is recommended.

The aim of the present study is to investigate the effects of altering the characteristics of the baseplate geometric parameters including stress distribution, torque resistance, and product deformation. The deformation is represented by a tilt angle measured between the baseplate plane and the actuator arm plane. In the current study, the ball swaging process is studied by performing a large-deformation dynamic finite element analysis (FEA) using a commercial program, ABAQUS (2008). The one-sided top arm in the assembly is opted as an example to be studied. The ball diameter is 2 mm and its velocity maintains constant at 60 mm/s in the top-to-bottom direction.

2. Finite element modeling and validation

The three parts involved in the swaging process, the arm, the baseplate and the suspension, are modeled. The problem is simplified into that of a two-dimensional axisymmetric analysis. Accordingly, a rectangular baseplate is modeled as a circular one and the effects along the length of the arm and the suspension are not considered. Normally, the length of the long arm has its own flexibility and acts as a spring support when the swaging ball comes in contact with the baseplate. The aforementioned assumptions are employed to simplify the analysis and optimize the computational cost with some penalties in accuracy of the displacement and stress fields. Results from the analyses and their comparisons are therefore assessed qualitatively, and not quantitatively, for the purpose of understanding the effects of each geometric parameter.

The FE model is depicted in Figure 3. Spacer keys used to separate the actuator beams from each other are simulated as rigid plates. Since the prototype arm is significantly longer than that in the simplified model and very stiff compared to other parts, fixed supports are applied to the cutout end of the arm. The contact surface between the suspension and the baseplate, which are welded together, is assumed as a glued surface. Two edge-to-edge contact pairs are imposed as frictional contact, viz., the surface between the swage ball and the swage boss and between the arm and the baseplate. The coefficients of friction for the former and the latter pairs are 0.6 and 0.25, respectively. These values are determined by tuning within the known ranges of

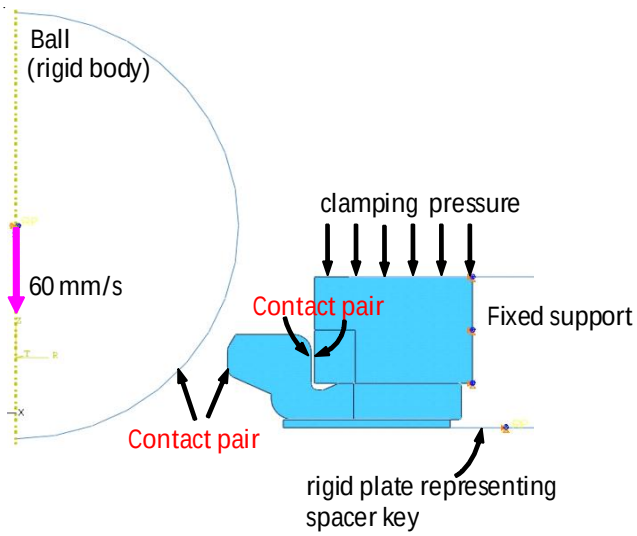

Figure 3. Loading and boundary conditions for the finite element model.

Table 1. Material properties used in the finite element analysis.

Material Properties	Type of Material	
	Stainless steel	Aluminum
Elastic modulus, E (MPa)	200,000	68,900
Yield stress, Y (MPa)	215	275.1
Poisson ratio	0.29	0.33
Mass density (kg/m^3)	7920	2700

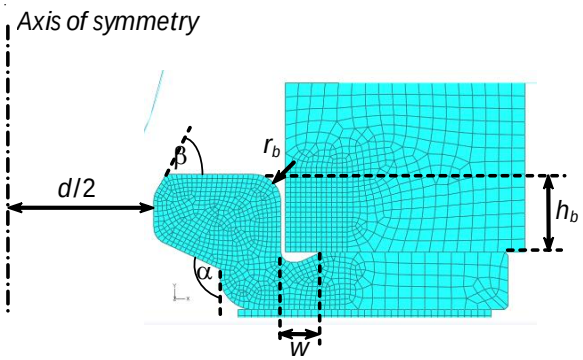

Figure 4. Meshing of the assembly and geometric parameters of interest.

frictional coefficients from 0.35 to 0.65 for the former pair and from 0.1 to 0.3 for the latter pair so that the retention torque of the assembly and the force occurred at the swage pin are in accordance with those obtained from the real situation.

The properties of the materials used in the analysis are listed in Table 1. Baseplate and suspension are stainless steel while the arm is made of aluminum. The material models defined in the analysis are strain-hardening Johnson-Cook model. The swage ball is made of stainless steel with hardened coating. In practice, the ball can be deformed and a new set of balls are needed after a few uses. In this analysis, the deformation is neglected and the ball is simulated as a rigid body.

Meshing of the structure is portrayed in Figure 4. All the elements used in the analysis are four-noded quadrilateral elements. To reduce computational time, the arm and the baseplate are partitioned such that fine meshes are only required in the vicinity of the contact areas and the elements are coarser in the areas farther away. The element sizes and the number of elements for each part are summarized in Table 2.

The analysis is performed through the following steps. First, a compressive clamping force of 588.6 N is applied to the rigid plate on top of the arm. Next, the swage ball is driven through the opening along the axis of symmetry with constant velocity of 60 mm/s. After that, the clamping force is released to allow final deformation. To reduce computational time a mass scaling factor of 10 is used. Results, including contact pressure profile and reaction force at the ball reference point, are evaluated. The stress distribution

Table 2. Element sizes and numbers of elements.

Part name	Fine meshing		Coarse meshing	
	element size (μm)	number of element	element size(μm)	number of element
Arm	15	204	40	359
Baseplate	15	757	40	92
Suspension	20	76	-	-

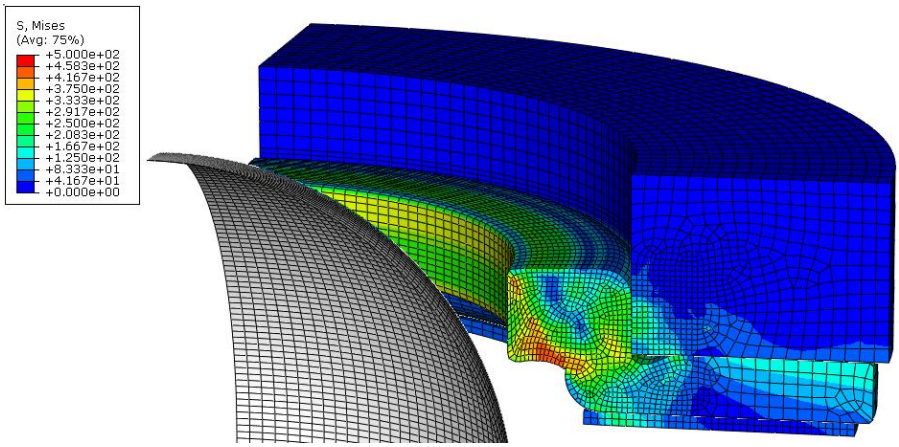

Figure 5. Stress distribution and deformed shape of the assembly after swaging process.

Table 3. Comparisons of prototype results obtained from measurements and FEA.

Results	Obtained value		Differences (%)
	Measurement	FEA	
Torque retention (N.m)	0.0981	0.0883	9.9
Peak force at swage pin (N)	212	227	7.1

and the deformed shape of the prototype assembly after the swaging process are shown in Figure 5. The deformed configuration is inspected to be in good agreement with factory samples.

Wadhwa (1996) suggested a simplified formula to calculate the retention torque, T, as

$$T = \mu r^2 \int_0^{2\pi} \int_0^{l} P(s) ds d\theta \quad (1)$$

where, r is radius of the arm opening, $P(s)$ is the contact pressure profile, l is the width of the contact area and the contact angle is 2π. Equation (1) can be modified as a discrete summation for FE results from an axisymmetric model as follows,

$$T = \pi \mu r^2 \sum_{n=1}^{N} \left((P_n + P_{n+1}) \Delta y_n \right) \quad (2)$$

where, the subscript n refers to the element number, N is the number of elements in contact, and Δy is the element dimension along the contact edge.

The accuracy of the model is validated by comparisons of the retention torque and the force occurred at the swage pin. Table 3 shows the differences between the average values obtained from ten measurements of factory samples and the results from FEA. The measurement of torque retention is achieved by destructive testing in which an increasing torque is directly applied to the suspension until the suspension is detached from the baseplate. The maximum torque is then read as the value of torque retention. The force at swage pin is gauged by a load cell attached to the pin tip and is compared to the maximum reaction at a reference point on the ball attained from the FEA. The differences are within 10% and could be the products of some other effects not considered in the present analysis, such as, misalignment of the centers of the ball and the swage hole, or uncertainties of the swage ball sizes and shapes.

3. Effects of geometric parameters

The results from FEA show that the characteristics of baseplate geometry have great influences on the quality of the attachment of the assembly parts. The effects of each geometric parameter are studied in the current work. Understanding of this matter would benefit in designing a proper figure of the baseplate corresponding to its design requirements. Six parameters as shown in Figure 4 are investigated. The examined variables are inner diameter of swage boss d, height of the baseplate h_b, angle of the first contact area at the top inner corner of the swage boss β, round radius at the inner corner of the boss r_b, width of the channel at the neck of baseplate w, and chamfer angle at the bottom of swage boss α.

3.1 Inner diameter of swage boss

The effects of changing the size of the swage boss inner diameter are inspected by the use of the ratio of the swage boss inner diameter d to the swage ball diameter D. Torque retention and tilt angle for the baseplate with a d/D ratio in the range of 0.92 to 0.97 are shown in Figure 6a. The stress distributions for such cases are illustrated in Figure 6b. For a d/D ratio of greater than 0.97, although the ball is still larger than the opening, the pressing force from the ball is not adequate to be transferred to the arm and failure of the swaged connection occurs. High retention torque and small tilt angle are achieved when the d/D ratio is 0.94. For smaller ratios, the ball goes through the hole with more difficulties and a high stress concentration at the bottom part of the

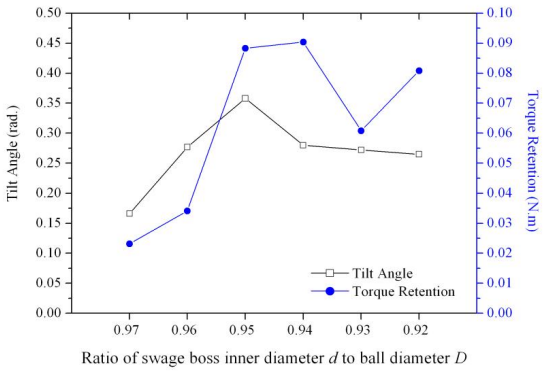

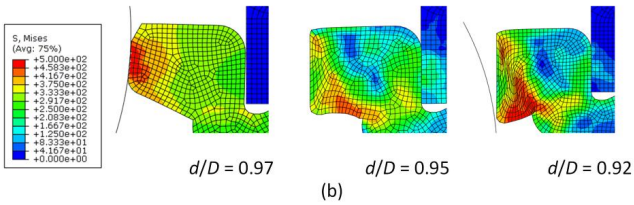

Figure 6. Results for different ratios of d/D (a) tilt angle and torque retention (b) stress distribution and deformed configuration.

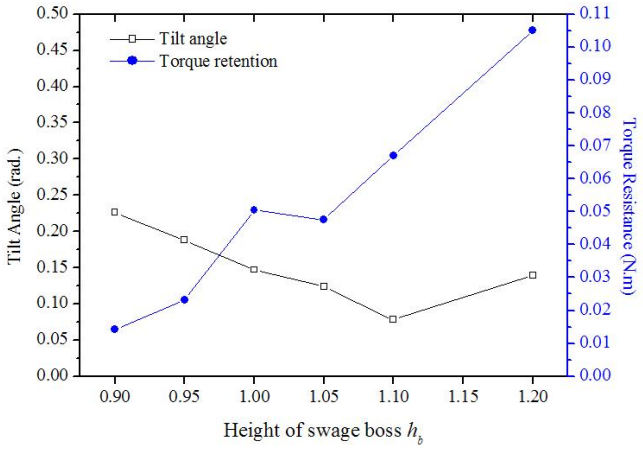

Figure 7. Tilt angle and torque retention for different boss heights.

swage boss is created. This causes the contact pressure between the suspension and the arm to be released to some extent and leads to lower torque resistances and small tilt angles.

3.2 Height of swage boss

To consider the effects of changing the height of the swage boss, a dimensionless parameter h_b, defined as the ratio of swage boss height to the height of the arm neutral axis, is varied from 0.9 to 1.2. For the ratio equal to unity, the top surface of the swage boss is at the level of the arm's neutral axis. Result from FEA in Figure 7 show the increase of torque resistance as well as the decrease of tilt angle as the height of the swage boss increases. This is due to both the larger contact area between the swage boss and the arm and the lower stress concentration at the neck of the baseplate. However, it should be noted that the ratio of greater than unity is only possible for the top or the bottom arm where only one suspension is attached to the arm.

3.3 Angle at the top inner corner of swage boss

The effect of varying the chamfer angle β from 15 to 90 degrees, while the height of the contact area between the ball and the boss remains the same, is inspected. Tilt angle and torque resistance are as shown in Figure 8a. Both values have been noticed to give similar tendency for all the cases. It can be seen from the FE results that this angle affects the area where the swage ball first contacts with the baseplate (Figure 8b). The optimum value for the angle? β is the one where the contact region goes along the ball surface. In this case, the optimum angle is 60 degrees. At this angle, the final shape of the inner part of the swage boss becomes straight although some angle is present at the beginning. Thus, the contact pressure profile distributes almost evenly over the contact region. In contrast, for a small angle β, the ball first contacts on the chamfer area and thus generates only stresses at the inner part of the boss. For a large angle β, the top element of the swage boss is shoved and pushed up later on

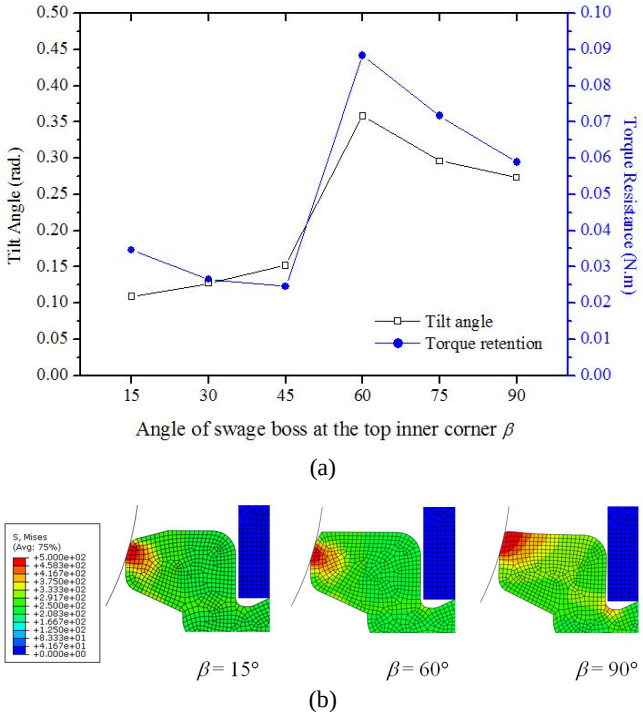

Figure 8. Results for different angle β (a) tilt angle and torque retention (b) area of the first contact between the ball and the boss.

as the ball is passing through due to excessive material of the part. For both of the latter cases, the stresses are exceedingly concentrated at the inner part of the boss but do not distribute to the arm and hence the retention torque between the baseplate and the arm becomes very low.

3.4 Round radius at the top outer corner of the boss

The round radius at the top outer corner of the boss r_b is varied from 16 to 144 μm. Results from FEA are depicted in Figure 9. It is observed that for small round radii, the

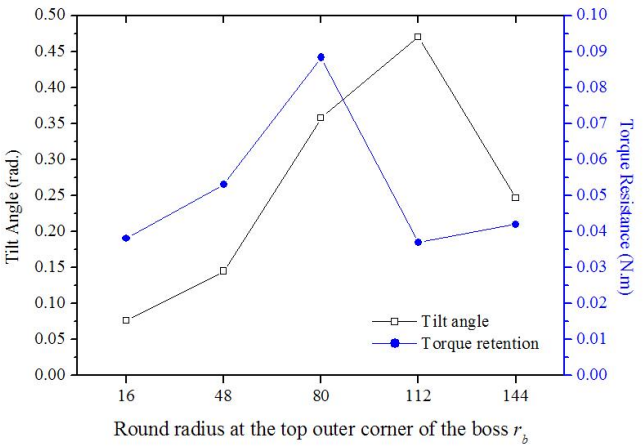

Figure 9. Results for different r_b (a) tilt angle and torque retention (b) stress distribution at the final stage.

contact area between the ball and the arm is limited only at the top part of the boss. Although the contact pressure is fairly high, merely a small amount of torque resistance is attained. A larger size of round radius contributes to a more evenly distributed pressure profile over the boss height. Nonetheless, outsized round radii reduce the contact area. In these cases, torque resistances are low as well as the product tilt angles. The case, which should essentially be avoided is one that the contact area is restricted to only the top part of the boss where it is too close to the neck, e.g., the case of r_b 112 μm. For this case, the torque retention is low while the occurred tilt angle is high due to stress concentration at the neck.

3.5 Width of the channel at the neck of baseplate

The channel at the neck of the baseplate is responsible for the relaxation of stress occurred at the necking. Distributions of normal stress in x-direction at the neck of the baseplate before the release of clamping pressure are shown in Figure 10a. A higher compressive stress concentration at this part is observed for narrow channels. This stress leads to a tilt angle of the baseplate when clamping pressure is no longer applied. The channel width w is studied for a range of 27 μm to 39 μm (Figure 10b). The optimum value for the present case is 33 μm.

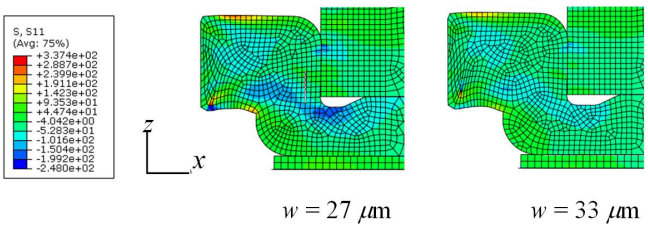

(a)

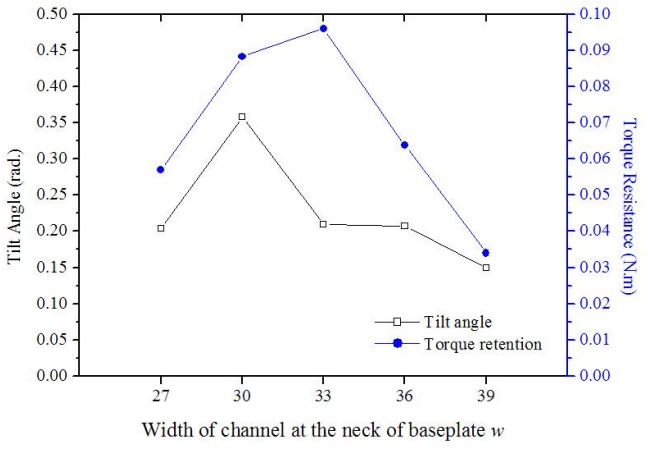

(b)

Figure 10. Results for different w (a) distribution of normal stress in x-directon (b) tilt angle and torque retention.

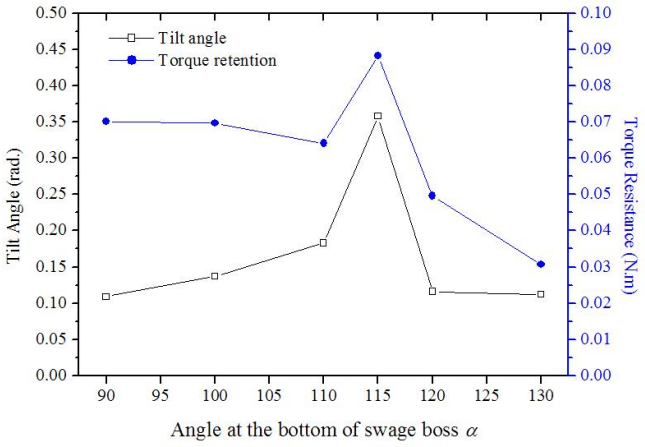

(a)

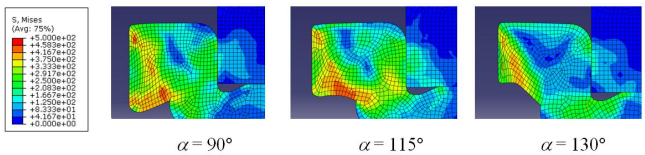

(b)

Figure 11. Results for different angle α (a) tilt angle and torque retention (b) final deformation.

3.6 Angle at the bottom of swage boss

Tilt angle and torque retention for angles at the bottom of the swage boss α ranging from 90 to 120 degrees are depicted in Figure 11a. Similar to other parameters, these two values show the same trend for all the studied cases. Final configurations for 90°, 115° and 130° are illustrated in Figure 11b. When the angle α is smaller than 110 degrees, excessive material at the bottom part of the boss induces compression between the boss and the baseplate flange. Force from the swage ball cannot be transferred to the arm. It can also be observed that when the angle α is large, the area of contact between the swage ball and the boss decreases. As a result, the contact surface between the boss and the arm is restricted leading to low torque retention of the connection. For the angle α of 115 degrees, the final shape of the boss cross-section after swaging process is almost rectangular. In this case, force transference from the ball to the arm is the most efficient. Hence, torque retention is the highest.

It should be noted that the numerical results for torque resistance and tilt angle presented in Figures 6 to 11 were obtained for each point shown in those figures. The straight lines connecting these points are for the purpose of comparison and tendency illustration. The relationship between the two quantities and the governing parameters could not be taken as linear relationships.

4. Baseplate geometry for improved torque retention

The baseplate is the part accountable for transferring

Table 4. Geometric parameters and results of proposed models.

Model	h_b /half arm height	w (μm)	d/D	Cross-sectional area (μm^2)	Tilt angle (deg.)	Torque retention (kN.m)
Prototype	0.9	30	0.95	225289	0.358	0.088
A	1.2	30	0.95	251658	0.186	0.106
B	1.2	33	0.95	251238	0.159	0.126
C	1.2	33	0.94	252560	0.158	0.137
D	1.2	30	0.94	252140	0.173	0.147

the force from the arm coil to move the suspension, thus the head slider, to its required position. For a hard disk drive to run properly, the swaged product must possess adequate torque retention to resist the torque occurred during the operation. Results from earlier analyses show that high torque resistance of a swaged product is achieved when high contact pressure at the surface between the swage boss and the arm is generated. For many cases, this is accompanied by an unfavorable large tilt angle. The outcomes of combinations of change in geometric parameter are therefore investigated so as to obtain the geometry of the baseplate with improved torque retention and decreased tilt angle.

The prototype, which was previously used in the FE validation, is presently employed as the basis of the design. The prototype already possesses angle β, angle α, and round radius r_b at the optimum values of 60°, 115°, and 80 μm, respectively. Model A to D are proposed by modifying the three remaining parameters one by one. The parameters, cross-sectional areas, and the results of all models are presented in Table 4. Figure 12 demonstrates a plotted graph between the tilt angle and the torque retention for each model. The intersection of the two axes is chosen to be at a point where torque resistance is high and no tilt angle is present. Therefore, the nearer the plotted result to the intersection, the better the quality of the swaged connection. It can be seen that performances of all proposed models are better than that of the prototype. The swage boss height h_b of model A is changed to the optimum value from earlier analysis of 1.2 times the arm neutral axis. This model yields higher torque resistance and considerably lower tilt angle as expected. The channel width at the neck of baseplate w is changed to 33 μm in model B and another 19% increase in torque retention and 15% decrease in tilt angle are achieved. All optimum values of geometric parameters as recommended in the previous section are applied in Model C and results show improvement of both values. When compared to the prototype, torque retention of model C is enhanced by 56% whereas the tilt angle is reduced by 56%.

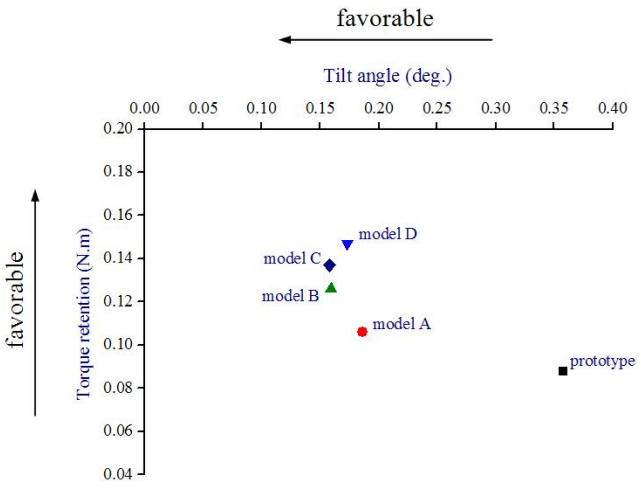

Figure 12. Tilt angle and torque retention of the proposed models.

A further investigation has been done by changing the width w to 30 μm while using d/D ratio of 0.94 in model D. This results in an even higher torque retention than that of model C. This verifies that combinations of optimum values may not always give rise to the best design. Some slight variations could be presented. Nonetheless, the result of larger tilt angle in model D compared to model C agrees well with the preceding result in Figure 10b. Hence, it is concluded that although the use of all optimum values may not guarantee the best results of all possible cases, it can be utilized as a reliable guideline to optimum design. It should also be noted that the cross-sectional areas of the proposed models require approximately 12% more material than the prototype. However, when compared with each other, cross-sectional areas of all suggested models (i.e., model A to D) are comparable.

5. Conclusions

In the current work, behaviors and characteristics of the baseplate after swaging process are studied by means of two-dimensional explicit dynamic finite element analysis. The effects of changing several geometric parameters of the baseplate to torque resistance and tilt angle are investigated and discussed. The recommended values for all parameters are combined to attain an optimum design of the baseplate with improved torque retention and less tilt angle. It can be concluded that a proper design of the baseplate should be one that the force from the driven swage ball can be distributed to the arm in a way that a consistent contact pressure profile between the boss and the arm is generated over the contact area. At the same time, to prevent the occurrence of an extreme tilt angle, stress concentration at the neck of

the baseplate should be diminished. These could be accomplished by opting for a design that final configuration of the boss cross-section of the swaged baseplate is an almost rectangle. In order to identify the final shape of the swaged baseplate before production, finite element analysis has been proved as an effective tool.

Acknowledgment

Technical supports from Hitachi Global Storage Technologies (Thailand) Co., Ltd. and the National Electronics and Computer Technology Center (NECTEC) are acknowledged.

References

ABAQUS, 2008. Version 6.7, Dassault Systemes Simulia Corp.

Aoki, K. and Aruga, K. 2007. Numerical Ball Swaging Analysis of Head Arm for Hard Disk Drives. Microsystem Technology. 13, 943-949.

Boutaghou, Z. and Budde, R.A. 1999. Base Plate with Improved Torque Retention. United States Patent No. US 5,896,646, April 1999.

Diewanit, I., Sittipongpanich, K., Chettaisong, T. and Thaveeprungsriporn, V. 2005. Baseplate Design for Reducing Deflection of Suspension Assembly by Swaging. United States Patent No. US 2005/0078407 A1, April 2005.

Jongpradist, P., Rotbunsongsri, R., Sukkana, C. and Sungtong, W. 2009. Parametric Study of Baseplate Geometry Using Finite Element Analysis. The Second International Data Storage Technology Conference, Bangkok, Thailand, May 13-15.

Kamnerdtong, T., Chutima, S. and Ekintumas, K. 2005. Effects of Swaging Process Parameters on Specimen Deformation. Eighth Asian Symposium on Visualization, Chiangmai, Thailand, May 23-27, 50.1-50.7.

Kant, R. and Stefansky, F.M. 2000. Baseplate design for the arm and suspension assembly for minimal gram-force and z-height variation, United States Patent No. 6,128,164, October 2000.

Wadhwa, S.K. 1996. Material Compatibility and Some Understanding of the Ball Swaging Process. Institute of Electrical and Electronics Engineers Transactions on Magnetics, 32(3), 837-1842.

Yim, P. 2002. Swage plate with protruded walls to increase retention torque in hard disk applications. United States Patent No. 6,417,994, July 2002

Zhang, Y., Linnertz, W. A., Fossum, R.E. and Sloun, S.J.V. 2006. Swaging-Optimized Baseplate for Disk Drive Head Suspension. United States Patent No. US 7,042,680 B1, May 2006.

Zhang, Y. and Wolter, R.R. 2008. Baseplate for a Disk Drive Head Suspension. United States Patent No. US 7,339,767 B1, March 2008.